Present-day radiative effect from radiation-absorbing aerosols in snow

Paolo Tuccella[1,2], Giovanni Pitari[1], Valentina Colaiuda[1,2], **Edoardo Raparelli[2,3]**, Gabriele Curci[1,2],

[1]Departement of Physical and Chemical Sciences, University of L'Aquila, 67010 L'Aquila, Italy.
5   [2]Center of Excellence in Telesensing of Environment and Model Prediction of Severe Events (CETEMPS), University of L'Aquila, Italy.
[3] Deptartement Information Engineering, Electronics and Telecommunications, Sapienza Università di Roma, Italy.

Correspondence to: Paolo Tuccella (paolo.tuccella@aquila.infn.it, paolo.tuccella@univaq.it)

Abstract. Black carbon (BC), brown carbon (BrC) and soil dust are the most important radiation absorbing aerosols (RAA).
10   When RAA are deposited on the snowpack, they lower the snow albedo causing an increase of the solar radiation absorption. The climatic impact associated to the snow darkening induced by RAA is highly uncertain. **The climatic impact associated to the deposition of BrC and dust on snowpack and its uncertainties were not reported in the IPCC 5th Assessment Report (AR5), therefore, the contribution of anthropogenic sources and carbonaceous aerosols to RAA radiative forcing (RF) in snow is not clear. Moreover, the snow albedo perturbation induced to a single RAA species depends on** 15   **the presence of other light-absorbing impurities contained in the snowpack. In this work, we calculated the present-day RF of RAA in snow starting from the deposition fields from a 5-years simulation with the GEOS-Chem global chemistry and transport model.** RF was estimated taking into account the presence of BC, BrC, and mineral soil dust in snow, simultaneously. Modelled BC and black carbon equivalent (BCE) mixing ratios in snow and the fraction of light absorption due to non-BC compounds (f_{non-BC}) were compared with worldwide observations. We showed as BC, BCE and f_{non-} 20 $_{BC}$, obtained from deposition and precipitation fluxes, reproduce the regional variability and order of magnitude of the observations. Global average all-sky total RAA, BC, BrC and dust snow RF were 0.068, 0.033, 0.0066, and 0.012 W/m^2, respectively. At global scale, non-BC compounds accounted for 40% of RAA snow RF, while anthropogenic RAAs contributed to the forcing for 56%. With regard to non-BC compounds, the largest impact of BrC has been found during summer in the Arctic (+0.13 W/m^2). In the middle latitudes of Asia, the forcing from dust in spring accounted for the 50% 25   (+0.24 W/m^2) of the total RAAs RF. Uncertainties in absorbing optical properties, RAA mixing ratio in snow, snow grain dimension, and snow cover fraction resulted in an overall uncertainty of -50%/+61%, -57%/+183%, -63%/+112%, and -49%/+77% in BC, BrC, dust and total RAAs snow RF, respectively. **Uncertainty upper bounds of BrC and dust were about 2 and 3 times larger than the upper bounds associated to BC. Higher BrC and dust uncertainties were mainly due to the presence of multiple absorbing impurities in the snow. Our results highlight that an improvement of the** 30   **representation of RAAs in snow is desirable, given the potential high efficacy of this forcing.**

1 Introduction

In the last decades, many studies have recognized the radiation-absorbing aerosols (RAA), in particular black carbon (BC), brown carbon (BrC) and dust, to contribute to the climate warming once deposited on the snow and ice pack (Hansen et al., 2004, 2005, 2007; Flanner et al., 2007, 2009; Bond et al., 2013; Boucher et al., 2013; Lin et al., 2014; Pitari et al., 2015; Skiles et al., 2018). Observations show that the extent of snow coverage is declining, due to global warming (Sturm et al., 2017). RAAs deposition on snowy surfaces results in an enhancement of the absorbed solar radiation in snow, due to the snowpack albedo reduction. This process increases melting and therefore reduces the snow duration. As a result, the alteration of runoff timing and magnitude due to the climate warming is amplified (e.g., Coppola et al., 2014) with significant impact on water resources (e.g.; Painter et al., 2010; Skiles et al., 2012; Wu et al., 2018). Forcing efficacy by RAAs in snow is about three time larger than the forcing that results from carbon dioxide (CO_2) (Flanner et al., 2007; Bond et al., 2013; Boucher et al., 2013). However, the climatic effect associated to RAAs in snow is still highly uncertain.

BC is emitted by the incomplete combustion of fossil fuel (FF), biofuel (BF) and biomass burning (BB) (Bond et al., 2013), and is characterized by high efficiency in absorbing the incoming solar radiation (Bond et al., 2013; Boucher et al., 2013). Current estimates suggest BC as the second most important climate forcing species after carbon dioxide (Gustafsson and Ramanathan, 2016). A large regional variability in BC mixing ratio in snow, ranging over four orders of magnitude, has been found by Warren (2018). As an example, Doherty et al. (2010) reported values of 1-4 ng/g in Greenland ice sheets, 4-10 ng/g in the Arctic Ocean, 8-14 ng/g in Canada and up to 10-60 and 20-60 ng/g in Russian Arctic and Scandinavia. As for middle latitudes, BC mixing ratio in snow was found to be in the range of 5-70 ng/g in central North America (Doherty et al., 2014), 20-600 and 30-2000 ng/g in Northwest and Northeast China (Ye et al., 2012; Wang et al., 2013). The lowest BC mixing ratios in snow were founded in Antarctica, being in the order of tenths of ng/g (Warren and Clark, 1990; Grenfell et al., 1994; Zatko and Warren, 2015). Currently, the best estimation of the present-day radiative forcing (RF) by BC in snow and in melting snow-free sea ice is +0.040 W/m² (+0.01/+0.09 W/m²) and +0.012 W/m² (+0.008/+0.017 W/m²) (Bond et al., 2013), respectively. The change in the surface temperature global average resulting from the RF exerted by BC in snow ranges from +0.06 to +0.20 K, while equilibrium change in Arctic surface temperature is estimated to be in the range of 0.50-1.6 K (Bond et al. 2013, Flanner et al. 2007).

RAAs in snow are not only represented by BC, since the presence of both soil dust and absorbing organic aerosol (OA). Measurements across the Arctic and central North America suggested that 20-50% of the sunlight absorption in the snowpack is due to non-BC RAA particles (Doherty et al., 2010, 2014), while in the Qilian Mountains the snow particulate absorption is dominated by non-BC compound (around 100%), according to Wang et al. (2013).

BrC is defined as the radiation-absorbing fraction of OA (Andreae et al., 2006; Laskin et al., 2015); it absorbs shortwave radiation with wavelengths less than 400 nm (Lukacs et al., 2007; Alexander et al., 2008; Chen et al., 2010; Arola et al., 2011; Kirchstetter et al., 2012). Sources of such absorbing organic matter are still uncertain; observations indicate that BrC is mainly

65   produced by BF combustion, BB, and ageing of secondary organic aerosol (SOA) (Bones et al., 2010; Hecobian et al., 2010; Arola et al., 2011; Updyke et al., 2012; Lambe et al., 2013; Laskin et al., 2015; Guang et al., 2016), while other sources are represented by some aqueous-phase chemical reactions in clouds (Zhang et al., 2017). BrC treatment is poor in current atmospheric models due to lack of mass and absorption observations. For this reason, OA is commonly treated as scattering and only few studies have investigated climatic impact of OA as BrC (Wang et al., 2014; Lin et al., 2014; Saleh et al., 2015;

70   Jo et al., 2016; Wang et al., 2018; Brown et al., 2018; Tuccella et al., 2020). **IPCC 5th Assessment Report (AR5) did not assess** the absorption of BrC in snow. To the best of our knowledge, the global RF due to the change of OA in snow from preindustrial time was calculated by Lin et al. (2014) only, who reported estimated values ranging from +0.0011 to +0.0031 W/m^2.

      Soil dust are emitted from arid and semi-arid regions (Choobari et al., 2013) and from soils disturbed by anthropogenic

75   activities (Tegen et al., 2004; Ginoux et al., 2012). The largest amount of dust in snow was found downwind from large sources (Skiles et al., 2018). Soil dust is much less absorbing than BC, however, it may dominate the RF in snow when present in very high concentrations. Although dust emissions have increased (Mahowald et al., 2010**) and the dust absorption has not a negligible effect on springtime Eurasian snow (Flannet et al., 2009; Skiles et al., 2018), AR5 did not discuss** the radiative forcing of dust in snow.

80   Some studies have shown that the presence of non-BC that absorbs impurities in snow reduces the influence of BC, especially in regions located downwind from large dust sources (Bond et al., 2013). Flanner et al. (2009) found that the dust deposition on the snowpack decreases the BC RF by 25% and, according to Bond et al. (2013), the role of dust in reducing BC RF ranges from 10% to 40%. Dang et al. (2017) reported regional-averaged albedo reductions due to RAAs of 0.009, 0.012 and 0.077 for fresh snow in the Arctic, North America, and China, respectively. Moreover, in the same regions, the albedo reductions

85   caused by BC only are 0.005, 0.005, and 0.031. The same authors have also estimated an increase of 20-40% of albedo perturbation in snow that did not contain non-BC RAAs. On the other hand, the presence of different light-absorbing impurities may also impact the BrC RF. Beres et al. (2020) found that the BrC deposition onto pure snow resulted in a more than twice local instantaneous RF, with respect to a case with dark snowpack. These results highlight the importance of taking into account the concentrations in snow of BC, BrC, and mineral soil dust simultaneously.

90   RF by snow RAAs is also affected by other uncertainties related to emissions, snow ageing, scavenging of the impurities in melting snow, parameterization for snow cover fraction (SCF), and absorption optical properties. The overall error associated with BC RF due to these single uncertainties is -73%/+117% (Flanner et al. 2007; Flanner et al. 2009; Bond et al., 2013). To the best of our knowledge, there are no studies which quantify all these uncertainties for BrC and soil dust at global scale.

      In this study, we performed a multi-year simulation of the RAA mass concentration with the global chemical and transport

95   model GEOS-Chem (Bey et al., 2001). **RAAs mass and their optical properties have been simulated using the most recent updates in terms of ageing, size distribution and absorption optical properties, inferred from observational constraints**

following our previous work (Tuccella et al., 2020). Starting from the GEOS-Chem output, we have diagnosed the mass mixing ratios of RAAs in snow and, subsequently, calculated the RF for different RAA species. In Section 2, we provided the description of modelling tools used in this study. In Section 3, the modelled RAA content in snow was compared with the available observations and the associated RF was, therefore, calculated, taking into account the simultaneous presence of BC, BrC, and dust in the snow. Moreover, seasonal and regional differences about the RF of each species have been explored. We also provided insights about the contribution of anthropogenic and carbonaceous compounds to the total RF. Finally, we discussed the uncertainties in modelling this kind of forcing associated with the assumptions of RAA optical properties, RAA mixing ratio uncertainty, snow ageing, and snow cover fraction. The conclusions are given in Section 4.

2 Methods

2.1 GEOS-Chem model

Aerosol mass concentration was simulated with the GEOS-Chem global chemical and transport model, v11-01 (Bey et al.,
2001, with updates documented in www.geos-chem.org). Five years (2010 to 2014) were simulated by the model, with a grid
resolution of $4° \times 5°$ and 47 vertical levels up to 0.01 hPa. Herein, GEOS-Chem was driven by Modern Era Retrospective-
analysis for Research and Application version 2 (MERRA2) with assimilation of meteorological data from the Global
Modelling and Assimilation Office Goddard Earth Observing System (Rienecker et al., 2011).

**BC, BrC and dust are treated as described in Tuccella et al. (2020). BC emissions and ageing were considered as source-
dependent as in Wang et al. (2014, 2018) and hydrophobic and hydrophilic BC were tracked for FF, BF, and BB sources.
BrC was inferred from primary organic aerosols (POA) and secondary organic aerosols, while dust mass concentration
was simulated with a sectional approach and emitted dust size distribution following the function of Kok (2011). Larger
details about GEOS-Chem parameterizations and RAA treatment are provided in the Supplement.**

2.2 Snow albedo perturbation

The snow albedo reduction by RAAs was calculated through the parameterization of Dang et al. (2015), which is based on the
Mie theory for spherical particles (Mie, 1908) and assumes that snow impurities are externally mixed with snow grains. In this
scheme, the snow albedo reduction by BC is parameterized for three broad bands: all-wave, visible (VIS) and near-infrared
(NIR), by using a quadratic or cubic polynomial in BC mixing ratio, whose coefficients are themselves quadratic in snow grain
size (R_e). It should be noted that the parameterization of Dang et al. (2015) was formulated assuming a size distribution and a
complex refractive index for BC. Nevertheless, it can be used for BC particles with different size and refractive index, by
scaling the mass mixing ratio with the ratio between the mass absorption coefficient (MAC), based on own assumptions, and
the coefficient used in Dang et al. (2015). MAC of given aerosol species at a given wavelength λ is defined as:

$$MAC_\lambda = \frac{3Q_{ext,\lambda}(1-\omega_\lambda)}{4\rho R_{eff}}$$
(1)

where Q_{ext} is the extinction efficiency, ω the single scattering albedo, R_{eff} is the particle effective radius and ρ the particle
density. In our work, the contribution to snow albedo reduction from soil dust and BrC was taken into account through the
concept of black carbon equivalent (BCE) (Grenfell et al., 2011), following Ward et al. (2018):

$$BCE = BC + \sum_{i=1}^{4} \frac{MAC_{Dust,i}}{MAC_{BC}}[Dust_i] + \frac{MAC_{BrC_{BF}}}{MAC_{BC}}[BrC_{BF}] + \frac{MAC_{BrC_{BB}}}{MAC_{BC}}[BrC_{BB}] + \frac{MAC_{BrC_{SOA}}}{MAC_{BC}}[BrC_{SOA}]$$
(2)

being *[BC]* the BC snow mixing ratio, *[Dust$_i$]* the mixing ratio of dust in the dimensional *i*-th bin and *[BrC$_{BF}$]*, *[BrC$_{BB}$]*,
[BrC$_{SOA}$] the BrC mixing ratios from BF, BB and SOA sources, respectively. Once the BCE is calculated, the snow albedo
reduction from all absorbing impurities can be estimated with the parameterization for BC proposed by Dang et al. (2015). It

should be noted as the MACs that appears in the latter equation are spectrally averaged over an incident solar spectrum, which is characteristic of summer high-latitude conditions. MACs adopted in this work are discussed in the next subsections.

Dang et al. (2015) also provided a scheme for the albedo reduction of snow containing dust particles, gathered through an estimation of the BCE. However, this parameterization is not used in our work, for the following reasons: first of all, the scheme is based on assumptions about the refractive index and size distribution. In particular, in the Dang's scheme a single log-normal mode for long-range-transported dust is adopted, while, in our model, dust size distribution evolves in the time and is not log-normal. Secondly, our simulations included the coarsest dust particles founded near the sources and this aspect could not be well represented by the size distribution adopted by Dang et al. (2015).

Snow albedo is sensitive to grain size, which depends on snow aging processes (Flanner et al., 2006; Flanner et al., 2007). Many studies have considered R_e as a constant, while only few works used a physical model to calculate the R_e growth (Bond et al., 2013). Uncertainties in R_e resulted in an error of -42%/+58% in RF estimation (Flanner et al., 2007), for this reason and in order to take into account R_e seasonal and geographical variability, we used the exponential relationship proposed by Zhao et al. (2013) to calculate R_e, starting from the snow albedo inferred from MERRA2 reanalysis. It should be noted that this is a rough approximation, since the relationship of Zhao et al. (2013) was based on the snow reflectance measured near 1030 nm, while we use the snow broadband albedo in our work/experiment. Moreover, the relationship derived from the snow fields of the Heihe River Basin (China) could be not consistent in other regions.

Finally, impurity mixing ratios in snow were calculated as the ratio between the deposition fluxes of BC, dust, and BrC simulated by GEOS-Chem, and MERRA2 total precipitation flux (Kopacz et al. 2011; He et al., 2014). It should be highlighted as the impurity content in snow is not only determined by the accumulation rate from deposition processes, but it is also a function of the scavenged fraction of impurities by melting snow. According to Flanner et al. (2007), uncertainties in the scavenged fraction generate an error in BC RF estimation ranging between -31% and +8%.

2.3 Radiation-absorbing aerosol optical properties

In this work, we used the same set of optical properties for RAAs employed by Tuccella et al. (2020). The size distribution for BC is sources-dependent, according to Wang et al. (2018). The geometrical median radius was fixed to 30 and 70 nm for FF and BF/BB black carbon, while the standard deviations were 1.4 and 1.6, respectively. Following the recommendation of Bond and Bergstrom (2006), the applied refractive index was 1.95-0.79i. The BC density was assumed to be 1.8 g/cm^3. Using the Mie theory (Mie, 1908) and the resulting MACs at 550 nm were 6.3 and 6.2 m^2/g for FF and BF/BB BC, respectively.

The geometrical median radius, standard deviation and density of BrC are 90 nm, 1.6 and 1.3 g/cm^3, respectively (Wang et al., 2018). **The imaginary part of BrC refractive index has been inferred starting from the MAC of BF and BB absorbing OA reported by Wang et al. (2018). Larger details about this calculation are provided in the Supplement. Resulting MAC$_{BrC}$ at 440 nm were 1.56 for BF, 3.08 and 0.92 m^2/g for fresh and aged BB. Two different MAC$_{BrC}$ for freshly**

emitted and aged BB were used, with the aim of taking into account the blanching process of aged plumes, due to the photochemical ageing (Forrister et al., 2015). A MAC$_{BrC}$ of 0.3 m^2/g at 440 nm was assigned to BrC-SOA, as reported in Wang et al. (2014).

170   Dust optical properties were also inferred as in our previous work (Tuccella et al., 2020). GEOS-Chem simulates the dust size distribution over four dimensional bins (see Section 2.1), however, the finer bin was split into four bins, for optical calculations, as in Ridley et al. (2012). The refractive index for mineral dust particles was derived from the dataset provided by Petzold et al. (2009). Under these assumptions, Mie calculation indicates a MAC at 550 nm of 0.057 and 0.048 m^2/g for size range of 0.36–0.6 and 4.4–6.0 μm, which are representative of the dust particles laying far and close to the sources, respectively.

2.4 Numerical experiments

We carried out a series of numerical experiments, in order to study the sensitivity of RAAs snow RF, due to the i) simultaneous presence of several light-absorbing impurities; ii) their absorbing optical properties; iii) their emissions and mixing ratios in snow; iv) snow grain size and v) snow coverage fraction. The list of our experiments is reported in Table 1.

The first simulation performed represented our reference case (CTRL), where a simultaneous presence of BC, BrC is
180   considered in the snow. The absorption enhancement (E$_{abs}$) of BC due to the "lensing effect" (Lesins et al., 2002), caused by coating of non-absorbing material, was taken into account increasing the MAC of aged (hydrophilic) BC, by a 1.5 factor, as recommended by Bond et al. (2013). We considered the CTRL simulation as the "central" (or "mid") absorption scenario. MACs averaged in the VIS are listed in Table 2, while those adopted for NIR are reported in Table S1.

In the second simulation, the RF of each single species at time (OSPT) in snow was calculated. The experiment main purpose
185   was to test how much the presence of more RAAs in snow affects the RF of a single species.

The six perturbed experiments were aimed at evaluating the sensitivity of RF to the assumed absorption aerosol properties. For these experiments, we defined a "high" and a "low" absorption scenario for absorbing aerosol species. Estimation of coated E$_{abs}$ is highly uncertain; recent studies have found values above the most accepted amount of 1.5. Tuccella et al. (2020) reported values in the range of 1.7–1.9 for BC coated by non-absorbing shell. According to the same authors, E$_{abs}$ is 2.8-3.4 for BC
190   coated by an absorbing shell (brown carbon). Curci et al. (2019) also estimated similar values. On the other hand, E$_{abs}$ values could be lower than 1.5, as an example, Cappa et al. (2012) have observed very low values for E$_{abs}$ (about 1.1). As a consequence, we applied E$_{abs}$ of 1.9 and 1.1 for BC "high" (BC-H) and "low" (BC-L) absorption scenario, respectively.

MAC adopted for BrC has been optimized with regional observations in the United States (Wang et al., 2018), therefore, assumed values/estimation may be not consistent worldwide. MAC used for aged BB BrC were deduced from limited dataset
195   (Wang et al., 2016), not able to provide the most required constraints on the photochemical whitening processes (Wang et al., 2018). Moreover, it is not clear if the blanching processes affects the BF BrC, for this reason, two extreme conditions for BrC absorption have been tested. In detail, a no whitening process for aged BB BrC was assumed in "high" absorption scenario

(BrC-H), while the whitening of BF BrC is considered in "low" absorption scenario (BrC-L). In the latter one, we assumed that MAC of aged biofuel BrC is reduced by a factor of 2.34 with respect to CTRL run.

Soil dust absorption and its climatic impact strongly depends on the imaginary part of the refractive index (Pitari et al., 2015; Tuccella et al., 2020), which is determined by the mineral composition of soil in the source region. Herein, we have explored the sensitivity of dust absorption in the snow due to the refractive index. In particular, the dataset of Wagner et al. (2012) was exploited for the "high" absorption simulation (DUST-H), while the refractive index from Sinyuk et al. (2003) was used in the "low" absorption experiment (DUST-L). As shown in Table 2, the considered dust size ranges of MACs are larger up to 3.5 times in DUST-H, with respect to CTRL. By contrast, MACs of DUST-L are lower up to a 1.6 factor, with respect to the reference simulation.

Two of the perturbed experiments were aimed at evaluating the sensitivity of RAAs snow RF to their concentration in the snowpack. The mixing ratio of absorbing impurities in the snow depends on many factors, such as emissions, deposition and precipitation rates, impurities solubility and snow melting (Flanner et al. 2007; Bond et al., 2013). Previous studies had shown that BC absorption is underestimated in GEOS-Chem and this was partly related to the uncertainties in both anthropogenic and biomass burning emission inventories (Wang et al., 2014; Jo et al., 2016; Tuccella et al., 2020). Data analysis and modelling revealed that current inventories underestimate the emissions from shipping and petroleum extraction in the Arctic (Tuccella et al., 2017; Law et al., 2017). On the other hand, dust emission is also uncertain. As an example, Kok et al. (2017) reported a range of values within 1000-2700 Tg/yr, for global PM_{10} dust, based on observational constraints. Furthermore, another uncertainty factor that affects our simulations, is associated to the fraction of POA emission we assumed as BrC. In order to evaluate the impact of all these uncertainties in snow RF calculation, we perturbed the RAA mixing ratios in snowpack by doubling (BCE-H) and halving (BCE-L) the BCE.

The last two experiments were performed to test the sensitivity of RAA-snow RF to R_e and SCF. As explained in the Subsection 2.2, we have estimated R_e with a rough method starting from the broad band snow albedo derived from MERRA2 data. In order to explore the impact of uncertainties in RAA snow RF related to R_e estimation, we multiplied (R_e-H) and dived (R_e-L) the snow grain radius by a factor 2.

SCF controls the area where RAA snow RF acts. In models, SCF is usually calculated using the snow depth (Flanner et al., 2007; Bond et al., 2013). According to Flanner et al. (2007), SCF may differs up to a factor of 2 among the various parameterizations, resulting in an uncertainty of -17%/+8% in BC snow RF (Bond et al., 2013). In MERRA2, SCF fraction is parameterized as a function of the snow water equivalent (SWE) (Rienecker et al., 2011). In order to evaluate how SCF uncertainty impacts the RAA snow RF, SWE has been multiplied (SCF-L) and divided (SCF-H) by a factor of 1.5.

2.5 Radiative transfer model

RAA-snow RF due to snow albedo reduction was calculated with the Rapid Radiative Transfer Model for General Circulation Models (RRTMG) (Iacono et al., 2008). RRTMG was interfaced with GEOS-Chem output and MERRA2 data as described by Jo et al. (2016) and Tuccella et al. (2020). Aerosol optical properties used for the atmospheric radiative transfer were calculated using the post-processing tool FlexAOD (Curci et al., 2015; Curci et al., 2019).

3 Results and discussion

3.1 Model evaluation

235 BC and BCE mixing ratios in snow diagnosed from GEOS-Chem deposition fields have been compared with the worldwide observations reported in different works. For Arctic and North America, we used the data from Doherty et al. (2010, 2014). For China, we inferred the measurements from Ye et al. (2012) and Wang et al. (2013), while for Himalya and Tibet Plauteau the observations were taken from Kopacz et al. (2011). Data for Antarctica were provided from Grenfell et al. (1994), Chylek et al. (1987), Warren and Clarke (1990), and Zatko and Warren (2015).

240 In Figure 1, the scatter plot obtained from the comparison between observed and simulated BC mixing ratios in snow surface layer is reported. In addition, results from the comparison are summarized in Table S2. Model simulations were compared to the observed regional median and standard deviation, provided in the reference papers. Where this information was not available, the analysis was carried out by considering the observed regional mean, together with the minimum and maximum values measured in the region of interest. When measurements corresponded to a specific period falling within the time interval

245 of our simulations (2010-2014), we had compared the model results for the same time frame. In other cases, the 5-year average over the same months has been used.

The R^2 coefficient between observed and calculated BC mixing ratios was 0.84. This result indicates as the regional variability of BC in snow, spanning over 5 order of magnitudes, is reproduced by the model. Most part of modelled values (80%) was found to drop within a factor of 2 from the observations. This last outcome reflects the model skill in reproducing both the

250 long-range BC transport and the impact of local major sources on the regional snow darkening. In general, the median bias of the modelled BC was -13%.

As for the Arctic, a significant bias was found in Greenland, during summer: in this area, modelled BC is about 7 times larger than the observed median mixing ratio. As discussed in Doherty et al. (2010), BC concentration in Greenland in summertime is larger in the melting layer (around 10 cm depth), with respect to the surface, as BC is left on the surface by the melted water.

255 Since this process is missing in the calculation schemes, it likely explains the obtained model bias in this case. In Eastern Russia, the modelled regional median was underestimated by a factor of 3. This bias could be related to both measurement uncertainties and model prediction. In fact, in some sites of Eastern Russia, BC measurements were affected by local soil dust and assumptions about the Ångström absorption exponent (AAE), which are made for the BC and non-BC components derivation in snow samples (Doherty et al., 2010). Moreover, some samples were not representative of the regional background,

260 because they were affected by local sources from villages (domestic wood-burning) and coal-fired power plants (Doherty et al., 2010), which could not be properly resolved by GEOS-Chem, given the raw resolution used in this work.

As for Antarctica, the model reproduced observed BC amount in snowpack and sea ice, except for Simple Dome station, where the mixing ratio is underpredicted by one order of magnitude. A similar bias was reported by Flanner et al. (2007), although the authors had used a most advanced scheme to calculate BC content in snow. Moreover, the BC concentration measurement

265   at Simple Dome (Chylek et al., 1987) is old (1982-1985) and may be not representative of the present-day Antarctic BC in snow, being much larger than more recent observations (0.20-0.60 ng/g), shown in Table 3.

The highest BC mixing ratios in snow are observed in China: the model reproduced the average magnitude of BC in snow detected in several regions of the country, with the exception of the industrial Northeast district. In this region, predicted BC concentrations are underestimated by a factor of 3, if compared to the typical values in the range of 1000-2000 ng/g in snow

270   surface (Wang et al., 2013). This area, where measurements reported by Wang et al. (2013) were collected (Table 3), hosts the highest number of industrial activities. As a consequence, the model negative bias found for this region may be another effect attributable to the adopted model resolution.

In Figure 2, the scatter plot resulting from the comparison between observed and simulated BCE (which is defined in Equation 2) mixing ratios in snow surface layer is shown. Numerical results are also reported in Table 3. The R^2 coefficient between

275   observed and calculated BCE mixing ratio was 0.60. As for BC, 80% of the modelled values were within a factor of 2 from the corresponding observations, resulting in a correct simulation of BCE regional variability. The median bias between observed and of modelled BCE was -21%: the highest BCE bias has been found in two regions of China, in particular, BCE is underpredicted by a factor of 3 in Qilian Mountains and Northeast Industrial region. By contrast, BCE resulted to be overpredicted by a factor of 3-4 in Greenland during summer months. In this case, the analysis of the light fraction absorption

280   due to non-BC compounds (f_{non-BC}) revealed other aspects of the model skill in reproducing the RAA in snow, **in terms of biases related to the emissions, transport, and assumptions done for absorbing optical properties.**

In Figure 3, a comparison between calculated and observed f_{non-BC}. f_{non-BC} is proposed, where a R^2 of 0.44. is reported, as well as a 90% of the modelled values being within a factor of 2 from observations. Generally, f_{non-BC} was underestimated by the model, with a median bias of -17%. The highest bias has been found for seasonal snow in North America. Furthermore, a

285   factor 2-underestimation of f_{non-BC} has been found in Intramountain Northwest (Rocky Mountain), Northern U.S. Plains (North Dakota), and Canada. In this case, it should be underlined as most part of the sites in Intramountain Northwest and Northern U.S. Plains are characterized by thin and patchy snow, and, therefore, affected by soil dust emitted by local sources (Doherty et al., 2014). This feature is not resolved by the model, due to the raw resolution used. Soil dust particles also contributes to absorption in Canadian snowy sites, implying a long range transport (Doherty et al., 2014) which is not simulated by GEOS-

290   Chem, being some local sources probably missing in the model.

f_{non-BC} was underestimated by a factor of 2 in Greenland during spring. In this period, snow RAAs in this country is usually dominated by biomass burning (Doherty et al., 2010), therefore, the f_{non-BC} bias is likely attributable to the BrC treatment in the model. Moreover, the simulated underestimation could be associated to the POA emissions from BB, as well as the absorption optical properties assumed to scale aged BB BrC mass in BCE calculation. Finally, in western Russia, the

295   underestimation of BC resulted in a highly biased f_{non-BC} (factor 1.5).

In summary, the model evaluation through worldwide observations showed a model skill in reproducing BC and BCE mixing ratios in snow. Obtained biases were mainly linked to the emissions of BC, POA, and dust emissions, while error in BCE and f_{non-BC} simulations was likely related to the assumptions about the RAA optical properties. A source of uncertainty in model evaluation could be represented by measurement errors. For example, according to Doherty et al. (2010), margins of error in BC and BCE measurements are related to both instrumental errors and assumptions made on the aerosol absorbing optical properties, which results in a total uncertainty estimation up to ±50%.

3.2 Present-day global radiative forcing

In Figure 4, the spatial pattern of the annual surface RF present-day average (2010-2014) from all RAAs, BC, BrC, and dust in snow is shown, as estimated from CTRL run and in all-sky conditions. In the following discussion, anthropogenic RAAs were considered as particles emitted by FF and BF sources and SOA formed by light photooxidation of aromatic compounds. BC and BrC from BB and biogenic SOA were considered as natural. Soil dust was also considered as a natural aerosol, even though about 20-25% of the total present-day emissions are attributed to human activity (Ginoux et al., 2012); these anthropogenic dust sources were not taken into account in this analysis.

Global average RF associated to all RAA was +0.068 W/m^2. The largest values were founded in Northeastern China and Tibet Plateau. As expected, global RAA-snow RF was dominated by BC RF, resulting in +0.033 W/m^2. This value is about 18% lower than the best estimation of 0.040 W/m^2, reported by Bond et al. (2013). In Figure S1, RF of BC, divided by source, is shown. About 80% (+0.025 W/m^2) of BC-snow RF was due to the anthropogenic sources. FF BC in snow RF acts everywhere, especially in Southeastern Canada, Eastern Greenland, Northeastern China, and Tibet Plateau. BF BC **showed** an impact in Eastern Europe, Northeastern China and Tibet Plateau. Eventually, BC from biomass burning occurred in Siberia and high latitudes, as a consequence of the boreal fires.

In our model, soil dust is the second light absorber in snow, having an average RF of +0.012 W/m^2 which was about 3 times lower than the radiative forcing due to BC. RF of dust in snow was relevant in the Asian regions, especially downwind the deserts and Tibet Plateau, where values up to +1.7 W/m^2 are simulated. In some regions of Kazakhstan, Mongolia, Manchuria, Tibet Plateau, Pakistan, and Afghanistan dust-snow RF is on average 2-3 times larger than what exerted by BC. In Mongolia, dust RF is up to 4 times larger than BC.

Estimation of snow RF for BrC was +0.0066 W/m^2, about 5 times lower than what calculated for BC. Lin et al. (2014) had reported values of 0.0011-0.0031 W/m^2 for RF of BrC in snow, as a result of an OA emission change of 60 Tg/yr since the preindustrial time. Starting from this RF, normalized to the emission change, the present-day RF may be estimated by using the current OA emission (124 Tg/yr) used in Lin et al. (2014). According to this scaling, the resulting RF was 0.0020-0.0055 W/m^2, therefore our estimation was above previous upper bounds. In Figure S2, the snow RF of BrC, divided by source, is displayed. BF BrC radiative effect was relevant in Northeastern China and Tibet Plateau, while BB BrC was dominant at high latitudes. Based on our model, BF and BB contribution to annual BrC snow RF was about 38% (+0.0025 W/m^2) and 47%

(+0.0031 W/m^2), respectively. SOA accounts for 15% (+0.0010 W/m^2) of OA absorption and its effect is limited at high latitudes in late spring and summer.

It should be noted as the sum of BC, BrC, and dust-snow RF is lower than the forcing of all RAAs. Albedo reduction does not increase linearly with the addition of RAAs, because the light that penetrates in the snowpack decreases as RAA concentration increases (Dang et al., 2017). As a consequence of this non-linearity, it is not straightforward to calculate the relative contribution of each absorbing impurity to total RF. An estimation may be given through the sequential factor separation analysis (Schär and Kröner, 2017); according to this method, non-BC compounds account for about 40% of the absorption in snow. In addition, we found that carbonaceous aerosols (BC+BrC) control about 75% (+0.046 W/m^2) of snow RF exerted by RAAs. The contribution of anthropogenic emissions to RAA absorption in snow is around 56% (+0.031 W/m^2), meaning that slightly less than half of RAA snow forcing is due to natural sources.

Total RAA-snow RF estimated in this study is about 6-7 times lower than the direct radiative effect exerted by RAAs (+0.36 and +0.10 W/m^2 for BC+BrC mixture and dust, respectively), calculated in our previous study (Tuccella et al., 2020). However, comparing RAA forcings in atmosphere and in snow by scaling them with their efficacies (Hansen et al., 2005), they are of the same order of magnitude. Forcing efficacy for BC in snow has been estimated 3 times larger than the one resulting from CO$_2$ (Flanner et al., 2007; Bond et al., 2013; Boucher et al., 2013). Assuming that the same efficacy is valid for both BrC and dust, the effective present-day RF from RAA in snow obtained in this study is +0.20 W/m^2. The atmospheric forcing estimated in Tuccella et al. (2020) may be scaled with the efficacies reported by Hansen et al. (2005), resulting in a total RAA effective forcing near +0.30 W/m^2.

3.3 Present-day regional and seasonal radiative forcing

In this section, a further investigation on the regional and seasonal dependence of RAAs-snow RF is proposed. To this aim, the globe has been divided into five regions, as defined in Table 4. In Figure 5, RF values from RAAs in snow at regional scale are represented as a function of season. The same figure also reports the relative contribution of each species to total RF.

In Arctic, total RAA-snow RF was +0.83 and +0.59 W/m^2 in spring and summer, respectively: about 40% of this forcing was attributable to non-BC compounds. According to our model, BrC contributed for the 14% to the total absorption in spring and reached the maximum values (+0.13 W/m^2) in summer, where the 32% of overall RAA RF is concentrated. BrC RF is higher in spring, especially on the snow land of Siberia and European high latitudes (**Figures S3, S4, S5**). This forcing is linked to both BF and BB sources. During summer, BrC RF is dominated by BB, as SOA accounted for about 13% (+0.017 W/m^2) of BrC forcing. By contrast, soil dust-snow RF has been found to be maximum in spring (+0.12 W/m^2) accounting for the 24% of the total forcing, whilst its radiative impact in snow is negligible in summer. Dust RF in Arctic is limited to the spring months during Arctic haze transport period, reflecting the absence of significant sources at high latitudes. Arctic dust absorption in springtime is important in Siberia, while minor impact was found in North America and sea ice (**Figure S6**). Moreover, about 60% of RAA snow RF in the Arctic was attributable to anthropogenic sources, in spring. In summer,

anthropogenic contribution dropped to 30%, as RF is dominated by BB. In fall, calculated RAA-snow radiative effect was +0.15 W/m^2, being 30% of this forcing due to non-BC aerosols, while 65% is determined by anthropogenic sources.

The lowest values of RAA-snow RF in the middle latitudes were found in North America, where the total RAA forcing resulted in 0.15 and 0.17 W/m^2 in winter and spring, respectively. In North-America, non-BC particles snow RF was the lowest obtained in our regional analysis. BrC and dust RFs **showed** a peak occurrence in spring, constituting the 13% (+0.014 W/m^2) and the 12% (+0.011 W/m^2) of the total forcing, respectively. RAA forcing was dominated by anthropogenic sources, 94% in winter and 77% in spring, nevertheless, non-BC forcing is likely underestimated. As discussed in Section 3.2, our model underestimated f_{non-BC} by about a factor of 2 in North America mountain regions, as local dust sources are missed in the model. As a consequence, dust forcing could be larger than estimations we reported in our analysis. Doubling BCE attributed to dust in North America, the corresponding RF increased by about 80%. Anthropogenic sources contributed for 94% and 77% to RAA forcing in winter and spring, respectively. However, anthropogenic impact should be reduced by increasing dust contribution to the forcing.

In the European continent, total RAA RF was +0.41 and +0.30 W/m^2 in winter and spring, respectively. BC absorption represented slightly more than half of the total forcing. BrC forcing was dominated by BF and located in Eastern regions over Europe (Figure S4). Absorbing OA contributed for about 10% of the total forcing (+0.027 W/m^2 in winter and +0.019 W/m^2 in spring). The largest non-BC compounds forcing was caused by soil dust. The radiative impact of dust was relevant in Eastern Europe and European Alps snowpack, where the dust snow RF was about 30%-40% of the total (+0.027 and +0.019 W/m^2 in winter and spring, respectively). Anthropogenic sources explained the 67% of European RAA-snow RF in winter: their contribution dropped to 58% in spring due to a larger influence of dust.

The largest RAA-snow RF values in the middle latitudes was found in Asia. In this area, RAA RF values were +0.56 and +0.64 W/m^2 in winter and spring, respectively. BrC contribution was constant (10%, about +0.033 W/m^2) between December and May. In particular, BF sources impacted the snow of North-eastern China, Kazakhstan, Southern Russia, and High Mountain, while BB determined some impact in Southern Siberia (Figure S4). Soil dust played a key role in Asia. According to our model, dust snow forcing was +0.10 and +0.24 W/m^2 in winter and spring, respectively. Spring dust forcing was larger than BC (+0.19 W/m^2) found in the same regions and constituted about a half of the total forcing. As a result, non-BC compounds gave the largest contribution (+60%) to RAA snow RF in Asia during spring. Dust particles caused the anthropogenic sources contribution to all RAA forcing to drop from 71% in winter, to 41% in springtime. Moreover, it should be noted as Asiatic RAA snow spatio-temporal averaged forcing was low in summer (+0.045 W/m^2), with relevant values in the High Mountain region, where it was up to 3 W/m^2. About 60% of this forcing was due to non-BC compound, while 10% and 50% is produced by BrC and dust, respectively. Middle latitudes of Asia are the only regions where the snow RAA is relevant in fall. In autumn, total RAA forcing was +0.19 W/m^2 and about half of this radiative effect is attributable non-BC compounds (10% and 40% to BrC and dust, respectively).

According to our model, the lowest RAA-snow radiative effect has been calculated in Antarctica. Here, the highest RF values have been found in winter and fall (austral summer and spring), as they were +0.14 and +0.11 W/m^2, respectively. The contribution of non-BC compounds was estimated to be 20-30% (10-20% is due to BrC and 10% if from dust), while anthropogenic sources impacted for the 68% and the 46% in winter and fall, respectively. The role of soil dust in Antarctica snow darkening could be underestimated in this study, as dust emission from arid regions of Southern Hemisphere calculated by our model was 65 Tg/yr. For the same Hemisphere, Ginoux et al. (2012) calculated an emission of 142 Tg/yr, half of which is linked to anthropogenic sources. This means that dust emission in Austral Hemisphere was underestimated in our simulations by a factor of 2, due to the missing of dust anthropogenic sources. As a result, the presence of anthropogenic dust in the model could have increased its role in Antarctica RAA-snow RF and have reduced the impact of anthropogenic compounds. Moreover, as discussed in Section 3.1, observations used to evaluate predicted RAA concentration in snow are obsolete and may be not representative of the current black carbon level in the Antarctica snow (see Table 3). The most recent measurements of BC, BCE and non-BC were carried out in 2012 (Zatko and Warren, 2015) and are relative to sea ice of East Antarctica. Although our modelled RAAs in snow are in agreement with these observations, this does not imply the same in other regions of Antarctica. As a consequence, it is difficult to establish the level of uncertainty of RF associated to the snow RAA concentration calculation.

3.4 Discussion of uncertainties

In this section, the impact of RAA in snow uncertainties on the RF is addressed. The impact of each single uncertainty was evaluated by comparing the perturbed experiments with CTRL simulation. Results are summarized in Table 3.

First, uncertainty of BC, BrC, and dust due to the presence of multiple radiation-absorbing impurities in the snowpack have been assessed. An increasing radiative effect, with respect to CTRL, was found when RF is calculated for one species at time (OSPT). According to our model, BC-snow RF increased by the 48% when BrC and dust are not present in the snow. This result is above the upper bound of 10-40%, estimated in previous studies (Flanner et al., 2009; Bond et al., 2013), where only the role of dust was considered in modulating the BC-snow RF. BrC forcing was enhanced by the 167% when black carbon and dust are in snowpack. This value is in line with Beres et al. (2020), where a reduction of local BrC RF of about a factor of 2 is reported, when the species is added to a dark snowpack. Finally, dust RF increased by the 92% in OSPT simulation.

Uncertainty associated to MAC of BC was -18% and +16% when an $E_{abs} = 1.1$ (BC-L) and $E_{abs} = 1.9$ (BC-H) are applied to the aged coated particles. The estimated range is comparable with those provided by previous works, where BC forcing uncertainty due to assumptions of its optical properties was estimated in the range ±12% (Bond et al., 2013). BrC forcing increased by 44% when the blanching of aged BB is missed (BrC-H). Taking into account a whitening process for BF (BrC-L), BrC-snow RF is lowered by the 22%. The uncertainty of soil dust RF associated to refractive index was -40% and +25% for DUST-L and DUST-H simulations, respectively.

Uncertainties in absorbing optical properties of a given species may also affect the forcing of other RAAs deposited on the
425 snowpack. When BC absorption was increased in BC-H experiment, BrC and dust forcing were reduced by about 10%.
Similarly, in BC-L simulation, the forcing of BrC and dust increased by the 10% and 5%, respectively. Uncertainty in BrC
absorption properties had a negligible effect (less than 5%) on BC and dust snow radiative effect. By contrast, the perturbation
to soil dust absorption optical properties (DUST-H and DUST-L) affected BrC-snow RF by about the 10%, however, the effect
on BC forcing was negligible. The estimated overall uncertainties in RF associated to the absorbing optical properties of
430 RAAs in snow were -18%/+17%, -27%/+45%, -41%/+25%, and -12%/+10% for BC, BrC, soil dust, and total RAAs snow RF.

Uncertainties related to RAA mixing ratio in snow obtained by halving (BCE-L) and doubling (BCE-H) the BCE, were -
36%/+50%, -44%/+44%, -35%/+40% for BC, BrC, and mineral dust, respectively. The uncertainty of total RAA snow forcing
due to BCE was -36%/+52%.

As for uncertainties linked to R_e (snow ageing), we found ranges of 30-36% for R_e-H and 22-27% for R_e-L. RAA snow RF
435 changes due to SCF perturbation were in the range of 22-30% and 11-20% for SCF-H and SCF-L, respectively. The overall
uncertainties in RF due to snowpack properties were -19%/+30%, -25%/+40%, -32%/+30%, and -31%/+46% for BC, BrC,
dust and total RAAs.

In summary, the estimated overall uncertainty in RF was -49%/+77% (0.035-0.12 W/m^2), -50%/+61% (0.017-0.059 W/m^2), -
57%/+183% W/m^2 (0.0028-0.019), -63%/+122% (0.0044-0.025 W/m^2), for total RAAs, BC, BrC, and dust, respectively. Total
440 uncertainties were calculated as the root sum of single squared errors, assuming that the single uncertainties are independent.
**Our results indicate that the lower bounds of total uncertainty of BC, BrC and dust were comparable. By contrast,
upper bounds for BrC and dust were about 2 and 3 times larger than the one of BC. According to our calculation, this
uncertainty was related to the simultaneous presence of multiple RAA species in the snowpack (OSPT experiment).**

Furthermore, it has to be highlighted as RAA snow RF can be affected by other uncertainties than what assessed in our study.
445 In particular, the cloud cover, which affects the incident solar radiation at surface and RAA optical properties in snow, that
also depends on the microlocation of impurities (i.e. if the aerosol particles are externally or internally mixed with snow grains).
In the second case, some authors estimated a BC absorption about 1.4-2.1 times larger, with respect to the external mixing
(Hansen et al., 2004; Flanner et al., 2012; He et al., 2014). Another uncertainty is related to the snow grain shape: non-spherical
grain assumption reduces the BC snow RF by 20–40% relative to spherical snow grains (He et al., 2014).

450

4 Conclusions

We presented a global modelling study to assess the present-day RF in snow due to the most relevant radiation-absorbing aerosols (BC, BrC, and dust). While BC RF in snow has been extensively studied (e.g., Bond et al. 2013; Boucher et al., 2013), the forcing from BrC and dust and associated uncertainties were not assessed in IPCC AR5, although they are recognised as radiation-absorbing particles. As a consequence, it is not clear what is the contribution of anthropogenic sources and carbonaceous aerosols to RAA-snow RF. Moreover, given that the snow albedo change is not linear with the impurity content (Flanner et al., 2009; Dang et al., 2017), RF from RAAs in snow has to be calculated taking simultaneously into account the concentrations of BC, BrC, and mineral soil dust.

Herein, we used the GEOS-Chem global chemistry and transport model to simulate BC, BrC, and dust deposition on the snowpack. The present-day radiative RF due to RAAs in snow was calculated considering the simultaneous presence in the snow of BC, BrC and dust. BC and black carbon equivalent (BCE) mixing ratios in snow were calculated starting from simulated deposition fields and precipitation fluxes. The obtained BC and BCE concentrations in the snowpack have been validated through worldwide observations. The model was able to reproduce the observed regional variations with a R^2 of 0.84 and 0.60 for BC and BCE, respectively. 80% of the modelled BC and BCE values were within a factor of 2 from the observations. The median bias for the same quantities was -13% and -21%. The model also reproduced the range of observed f_{non-BC} with a R^2 of 0.44 and a median bias of -17%.

According to the model, global annual mean present-day RAA-snow RF at surface was +0.037, +0.0064, +0.013, and +0.068 W/m^2 for BC, BrC, dust, and total RAAs, respectively. Non-BC compounds accounted for the 40% (+0.046 W/m^2) of RAA snow global RF and anthropogenic RAAs contributed for the 56% (+0.031 W/m^2) to the forcing.

At regional scale, RF exhibited large variability in terms of intensity and species apportionment. The largest total RAA-snow RF was found in Arctic during spring (+0.83 W/m^2) and summer (+0.59 W/m^2) and the 40% of this forcing was due to non-BC compounds. In particular, non-BC spring RF is mainly due to the dust (+0.12 W/m^2), while non-BC was driven by BB BrC (+0.13 W/m^2) in summer. In the middle latitudes, the most relevant RAA-snow forcing was obtained in Asia with +0.56 and +0.64 W/m^2 in winter and spring, respectively. BrC contribution was constant during winter and spring (10%, about +0.033 W/m^2), while soil dust exerted a key role in forcing over Asia: its radiative effect (+0.24 W/m^2) was larger than the one of BC and represented 50% of the total RAA RF in spring. RAA forcing on High Mountain region was up to 3 W/m^2 in summertime and 60% of it is attributable to non-BC aerosols. North America exhibited the lowest RAA-snow RF (0.15 and 0.17 W/m^2 in winter and spring, respectively) and the lowest non-BC contribution (about 20%) in the middle latitudes. As for Europe, total RAA RF was +0.41 and +0.30 W/m^2 in winter and spring, respectively. BC contributed slightly more than half of the total forcing. The most relevant non-BC was given by dust (30%-40% of the total). In Antarctica, the highest values of RF have been found in winter and fall (+0.14 and +0.11 W/m^2, respectively) and the contribution of non-BC compounds was estimated to be in the range of 20-30%.

In Arctic, the 60% of springtime RF was due to anthropogenic sources, while it dropped down to 30% in summer, due to BB.

485 In Asia, anthropogenic compounds contributed for the 71% to total forcing in winter, while the contribution was 41% in springtime, because of the presence of dust. A similar behaviour has been found in Europe, while in North America RAA-snow RF was always dominated by anthropogenic emissions.

Finally, we also explored the sensitivity of RF due to the simultaneous presence of multiple RAAs in snow, absorption optical properties, uncertainties in impurities mixing ratio, snow grain size and snow coverage. The overall uncertainty in RF

490 associated to these factors were -49%/+77% (0.035-0.12 W/m^2), -50%/+61% (0.017-0.059 W/m^2), -57%/+183% W/m^2 (0.0028-0.019), -63%/+122% (0.0044-0.025 W/m^2), for total RAAs, BC, BrC, and dust, respectively. **These results highlight that uncertainty upper bounds of BrC and dust were about 2 and 3 times larger than the one of BC. This uncertainty was mainly due to the simultaneous presence of multiple absorbing impurities in the snow. Therefore, we may conclude that RAA snow RF is very sensitive to the concomitant presence of more species, especially for non-BC compounds,**

495 **given their minor absorption with respect to BC.**

Efficacy of RF associated to BC in snow was 3 times larger than forcing from CO_2 (Flanner et al., 2007; Bond et al., 2013; Boucher et al., 2013). Assuming the same efficacy for BrC and dust, effective RF exerted by RAA in snow found in this study was +0.20 W/m^2, a value comparable with the RAA effective atmospheric forcing (about +0.30 W/m^2) obtained from Tuccella et al. (2020). Given that RF of RAAs in snow acts mainly on the cryosphere, it may potentially

500 **have important effects in response to the snow-albedo feedback. As a consequence, a reduction of the uncertainties is desirable. According to our results, a first step to reduce uncertainties in RAA-snow RF should be an improvement of the representation of RAAs in snow within models, through constraint with local and satellite observations and a better characterization of the emission inventories in current atmospheric models.**

505 **Code/Data availability:** GEOS-Chem simulations used in this study are accessible at this link https://osf.io/xntr8/. Snow impurity measurements are available in the paper referenced in the text. FlexAOD postprocessing tool can be provided upon request to gabriele.curci@aquila.infn.it. RRTMG code is available at this link http://rtweb.aer.com/rrtm_frame.html.

Author Contributions: Conceptualization, P.T., G.P.; Methodology, P.T.; Software, P.T., G.C., E.R.; Model simulations:

510 P.T.; Formal analysis, P.T., G.P., V.C.; writing–original draft preparation, P.T.; writing–review and editing, P.T., V.C., G.P., E. R., G.C.; project administration, V.C., P.T.; funding acquisition, P.T., G.C., and G.P.

Competing interests: The authors declare that they have no conflict of interest.

515 **Funding** Paolo Tuccella is beneficiary of an AXA Research Fund (2016-ENV-PostDoc-University of L'Aquila) postdoctoral grant. Valentina Colaiuda is supported by PON-AIM (PON-AIM1858058) program funded by Italian Ministry of University and Research (MUR).

520

Table A1. List of acronyms and symbols.

AAE	Absorption Ångström exponent
AOD	Aerosol optical depth
BB	Biomass burning
BC	Black carbon
BCE	Black carbon equivalent
BF	Biofuel
BrC	Brown carbon
DEAD	Dust Entrainment And Deposition
Eabs	Black carbon absorption enhancement factor
FF	Fossil fuel
FlexAOD	Flexible aerosol optical depth
MAC	Mass absorption coefficient
MERRA2	Modern Era Retrospective-analysis for Research and Application version 2
NIR	Near infrared radiation
OA	Organic aerosol
POA	Primary organic aerosol
R_e	Snow grain effective radius
RAA	Radiation-absorbing aerosol
RF	Radiative forcing
RRTMG	Rapid radiative transfer model for GCM
SCF	Snow cover fraction
SOA	Secondary organic aerosol
VIS	Visible radiation

References

525   Alexander, D. T. L., Crozier, P. A., Anderson, J. R: Brown carbon spheres in East Asian outflow and their optical properties, J. Geophys. Res., 321, 833–836, doi:10.1126/science.1155296, 2008.

Andreae, M. O. and Gelencsér, A.: Black carbon or brown carbon? The nature of light-absorbing carbonaceous aerosols, Atmos. Chem. Phys., 6, 3131–3148, https://doi.org/10.5194/acp-6-3131-2006, 2006.

Arola, A., Schuster, G., Myhre, G., Kazadzis, S., Dey, S., and Tripathi, S. N.: Inferring absorbing organic carbon content from 530   AERONET data, Atmos. Chem. Phys., 11, 215–225, https://doi.org/10.5194/acp-11-215-2011, 2011.

Beres, N. D., Sengupta, D., Samburova, V., Khlystov, A. Y., and Moosmüller, H.: Deposition of brown carbon onto snow: changes in snow optical and radiative properties, Atmos. Chem. Phys., 20, 6095–6114, https://doi.org/10.5194/acp-20-6095-2020, 2020.

Bey, I., Jacob, D. J., Yantosca, R. M., Logan, J. A., Field, B., Fiore, A. M., Li, Q., Liu, H., Mickley, L. J., Schultz, M.: Global 535   modeling of tropospheric chemistry with assimilated meteorology: Model description and evaluation, J. Geophys. Res., 106, 23073–23095, https://doi.org/10.1029/2001JD000807, 2001.

Bond, T. C., Bergstrom, R. W.: Light absorption by carbonaceous particles: an investigative review, Aerosol. Sci. Tech., 40, 27–67, doi:10.1080/02786820500421521, 2006.

Bond, T. C., Bhardwaj, E., Dong, R., Jogani, R., Jung, S. K., Roden, C., Streets, D. G., Trautmann, D. G.: Historical emissions 540   of black and organic carbon aerosol from energy-related combustion, Global Biogeochem., 21, 1850–2000, https://doi.org/10.1029/2006GB002840, 2007.

Bond, T. C., Doherty, S. J., Fahey, D. W., et al.: Bounding the role of black carbon in the climate system: A scientific assessment, J. Geophys. Res.-Atmos., 118, 5380–5552, https://doi.org/10.1002/jgrd.50171, 2013.

Bones, D. L., Henricksen, D. K., Mang, S. A., Gonsior, M., Bateman, A. P., Nguyen, T. B., Cooper, W. J., Nizkorodov, S. A.: 545   Appearance of strong absorbers and fluorophores in limonene-O3 secondary organic aerosol due to NH4+ mediated chemical aging over long time scales, J. Geophys. Res., 115, https://doi.org/10.1029/2009JD012864, 2010.

Boucher, O., Randall, D., Artaxo, P., Bretherton, C., Feingold, G., Forster, P., Kerminen, V.-M., Kondo, Y., Liao, H., Lohmann, U., Rasch, P., Satheesh, S. K., Sherwood, S., Stevens, B., and Zhang, X. Y.: Clouds and Aerosols, in: Climate Change 2013: The Physical Science Basis. Contribution of Working Group I to the Fifth Assessment Report of the 550   Intergovernmental Panel on Climate Change, edited by: Stocker, T. F., Qin, D., Plattner, G.-K., Tignor, M., Allen, S. K., Boschung, J., Nauels, A., Xia, Y., Bex, V., and Midgley, P. M., Cambridge University Press, Cambridge, United Kingdom and New York, NY, USA, 2013.

Brown, H., Liu, X., Feng, Y., Jiang, Y., Wu, M., Lu, Z., Wu, C., Murphy, S., and Pokhrel, R.: Radiative effect and climate impacts of brown carbon with the Community Atmosphere Model (CAM5), Atmos. Chem. Phys., 18, 17745–17768, https://doi.org/10.5194/acp-18-17745-2018, 2018.

Cappa, C. D., Onasch, T. B., Massoli, P., et al.: Radiative Absorption Enhancements Due to the Mixing State of Atmospheric Black Carbon, Science, 337, 1078–1081, https://doi.org/10.1126/science.1223447, 2012.

Chen, Y. and Bond, T. C.: Light absorption by organic carbon from wood combustion, Atmos. Chem. Phys., 10, 1773–1787, https://doi.org/10.5194/acp-10-1773-2010, 2010.

Chin, M., Chu, A., Levy, R., Remer, L., Kaufman, Y., Holben, B., Eck, T., Ginoux, P., Gao, O.: Aerosol distribution in the Northern Hemisphere during ACE-Asia: Results from global model, satellite observations, and Sunphotometer measurements, J. Geophys. Res., 109, https://doi.org/10.1029/2004JD004829, 2004.

Choobari, O. A., Zawar-Reza, P., Sturman, A.: The global distribution of mineral dust and its impact on the climate system: a review, Atmos. Res., 138, 152–165, https://doi.org/10.1016/j.atmosres.2013.11.007, 2013.

Chylek, P., Srivastava, V., Cahenzli, L., Pinnik, R. G., Dod, R. L., Novakov, T.: Aerosol and graphitic carbon content of snow, J. Geophys. Res., 92D8, 9801–19809, https://doi.org/10.1029/JD092iD08p09801, 1987.

Coppola, E., Verdecchia, M., Giorgi, F., Colaiuda, V., Tomassetti, B., Lombardi, A.: Changing hydrological conditions in the Po basin under global warming, Science of the total environment, 493, 1183-1196, https://doi.org/10.1016/j.scitotenv.2014.03.003, 2014.

Curci, G., Hogrefe, C., Bianconi, R., Im, U., Balzarini, A., Baro, R., Brunner, D., Forkel, R., Giordano, L., Hirtl, M., Honzak, L., Jimenez-Guerrero, P., Knote, C., Langer, M., Makar, P. A., Pirovano, G., Perez, J. L., San Jose, R., Syrakov, D., Tuccella, P., Werhahn, J., Wolke, R., Zabkar, R., Zhang, J., and Galmarini, S.: Uncertainties of simulated aerosol optical properties induced by assumptions on aerosol physical and chemical properties: an AQMEII-2 perspective, Atmos. Environ., 115, 541–552, https://doi.org/10.1016/j.atmosenv.2014.09.009, 2015.

Curci, G., Alyuz, U., Barò, R., Bianconi, R., Bieser, J., Christensen, J. H., Colette, A., Farrow, A., Francis, X., Jiménez-Guerrero, P., Im, U., Liu, P., Manders, A., Palacios-Peña, L., Prank, M., Pozzoli, L., Sokhi, R., Solazzo, E., Tuccella, P., Unal, A., Vivanco, M. G., Hogrefe, C., and Galmarini, S.: Modelling black carbon absorption of solar radiation: combining external and internal mixing assumptions, Atmos. Chem. Phys., 19, 181–204, https://doi.org/10.5194/acp-19-181-2019, 2019.

Dang, C., Brandt, R. E., Warren, S. G.: Parameterizations for narrowband and broadband albedo of pure snow and snow containing mineral dust and black carbon, J. Geophys. Res., 102, https://doi.org/10.1002/2014JD022646, 2015.

Dang, C.; Warren, S. G.; Fu, Q.; Doherty, S. J.; Sturm, M.; Su, J.: Measurements of light-absorbing particles in snow across the Arctic, North America, and China: Effects on surface albedo, J. Geophys. Res Atmos., 122, 10149–10168, https://doi.org/10.1002/2017JD027070, 2017.

Doherty, S. J., Warren, S. G., Grenfell, T. C., Clarke, A. D., and Brandt, R. E.: Light-absorbing impurities in Arctic snow, Atmos. Chem. Phys., 10, 11647–11680, https://doi.org/10.5194/acp-10-11647-2010, 2010.

Doherty, S. J., Dang, C., Hegg, D. A., Zhang, R., Warren, G.: Black carbon and other light-absorbing particles in snow of central North America, J. Geophys. Res., 119, 12807–12831, https://doi.org/10.1002/2014JD022350, 2014.

Flanner, M. G., Zender, C. S.: Linking snowpack microphysics and albedo evolution, J. Geophys. Res. Atmos., 111, https://doi.org/10.1029/2005JD006834, 2006.

Flanner, M. G., Zender, C. S., Randerson, J. T., Rasch, P. J.: Present-day climate forcing and response from black carbon in snow, J. Geophys. Res., https://doi.org/10.1029/2006JD008003, 112, 2007.

Flanner, M. G., Zender, C. S., Hess, P. G., Mahowald, N. M., Painter, T. H., Ramanathan, V., and Rasch, P. J.: Springtime warming and reduced snow cover from carbonaceous particles, Atmos. Chem. Phys., 9, 2481–2497, https://doi.org/10.5194/acp-9-2481-2009, 2009.

Flanner, M. G., Liu, X., Zhou, C., Penner, J. E., and Jiao, C.: Enhanced solar energy absorption by internally-mixed black carbon in snow grains, Atmos. Chem. Phys., 12, 4699–4721, https://doi.org/10.5194/acp-12-4699-2012, 2012.

Forrister, H., et al.: Evolution of brown carbon in wildfire plumes, Geophys. Res. Lett., 42, doi:10.1002/2015GL063897, 2015.

Giglio, L., Randerson, J. T., van der Werf, G. R.: Analysis of daily, monthly, and annual burned area using the fourth generation global fire emissions database (GFED4), J. Geophys. Res.-Biogeo, 118, 317–328, https://doi.org/10.1002/jgrg.20042, 2013.

Ginoux, P., Chin, M., Tegen, I., Prospero, J. M., Holben, B., Dubovik, O., Lin, S.-J.: Sources and distribution of dust aerosols simulated with the GOCART model, J. Geophys. Res., 106, doi:10.1029/2000JD000053, 2001.

Ginoux, P., Prospero, J. M., Gill, T. E., Hsu, N. C., Zao, M.: Global-scale attribution of anthropogenic and natural dust sources and their emission rates based on MODIS deep blue aerosol products, Rev. Geophys., 590, 50, https://doi.org/10.1029/2012RG000388, 2012.

Grenfell, T., Warren, S., Mullen, P.: Reflection of solar radiation by the Antarctic snow surface at ultraviolet, visible, and near-infrared wavelengths, J. Geophys. Res., 99D9, 18669–18684, https://doi.org/10.1029/94JD01484, 1994.

Grenfell, T. C., Doherty, S. J., Clarke, A. D., Warren, S. G.: Light absorption from particulate impurities in snow and ice determined by spectrophotometric analysis of filters, Appl. Opt., 50, 2037–1048, https://doi.org/10.1364/AO.50.002037, 2011.

Guang-Ming,W., Zhi-Yuan, C., Shi-Chang, K., Kawamura, K., Ping-Qing, F., Yu-Lan, F., Xin,W., Shao-Peng, G., Bin, L.: Brown carbon in the cryosphere: Current knowledge and perspective, Environ. Sci. Technol., 7, 82–89, https://doi.org/10.1016/j.accre.2016.06.002, 2016.

Guenther, A., Karl, T., Harley, P., Wiedinmyer, C., Palmer, P. I., and Geron, C.: Estimates of global terrestrial isoprene emissions using MEGAN (Model of Emissions of Gases and Aerosols from Nature), Atmos. Chem. Phys., 6, 3181–3210, https://doi.org/10.5194/acp-6-3181-2006, 2006.

Gustafsson, O., Ramanathan, V.: Convergence on climate warming by black carbon aerosols, P. Natl. Acad. Sci., 113, 4243–4245, doi:10.1073/pnas.1603570113, 2016.

Hansen, J., Nazarenko, L.: Soot climate forcing via snow and ice albedos, PNAS, 101 (2), 423-428; https://doi.org/10.1073/pnas.2237157100, 2004.

Hansen, J., Sato, M., Ruedy, R., Nazarenko, L., Lacis, A., Schmidt, G.A., Russell, G., Aleinov, I., Bauer, M., Bauer, S. et al.: Efficacy of climate forcing, J. Geophys. Res., 110, D18104, https://doi.org/10.1029/2005JD005776, 2005.

Hansen, J., Sato, M., Ruedy, R., Kharecha, P., Lacis, A., Miller, R.L., Nazarenko, L., Lo, K., Schmidt, G.A., Russell, G., et al.: Climate simulations for 1880–2003 with GISS, ModelE. Clim. Dyn., https://doi.org/10.1007/s00382-007-0255-8, 29, 661–696, 2007.

He, C., Li, Q., Liou, K.-N., Takano, Y., Gu, Y., Qi, L., Mao, Y., Leung, L. R.: Black carbon radiative forcing over the Tibetan Plateau, Geophys. Res. Lett., 41, 7806–7813, https://doi.org/10.1002/2014GL062191, 2014.

Hecobian, A., Zhang, X., Zheng, M., Frank, N., Edgerton, E. S., and Weber, R. J.: Water-Soluble Organic Aerosol material and the light-absorption characteristics of aqueous extracts measured over the Southeastern United States, Atmos. Chem. Phys., 10, 5965–5977, https://doi.org/10.5194/acp-10-5965-2010, 2010.

Iacono, M. J., Delamere, J. S., Mlawer, E. J., Shephard, W., Clough, S. A., Collins, W. D.: Radiative forcing by long-lived greenhouse gases: Calculations with the AER radiative transfer models, J. Geophys. Res., 113, https://doi.org/10.1029/2008JD009944, 2008.

Jo, D. S., Park, R. J., Lee, S., Kim, S.-W., and Zhang, X.: A global simulation of brown carbon: implications for photochemistry and direct radiative effect, Atmos. Chem. Phys., 16, 3413–3432, https://doi.org/10.5194/acp-16-3413-2016, 2016.

Kok, J. F.: A scaling theory for the size distribution of emitted dust aerosols suggests climate models underestimate the size of the global dust cycle, PNAS, 10, 274–281, https://doi.org/10.1073/pnas.1014798108, 2011.

Kok, J. F., Ridley, D. A., Zhou, Q., Miller, R. L., Zhao, C., Colette, L. H., Ward, D. S., Albani, S., Haustein, K.: Smaller desert dust cooling effect estimated from analysis of dust size and abundance, Nature Geoscience, 10, 274–281, https://doi.org/10.1038/ngeo2912, 2017.

Kirchstetter, T. W. and Thatcher, T. L.: Contribution of organic carbon to wood smoke particulate matter absorption of solar radiation, Atmos. Chem. Phys., 12, 6067–6072, https://doi.org/10.5194/acp-12-6067-2012, 2012.

Kopacz, M., Mauzerall, D. L., Wang, J., Leibensperger, E. M., Henze, D. K., and Singh, K.: Origin and radiative forcing of black carbon transported to the Himalayas and Tibetan Plateau, Atmos. Chem. Phys., 11, 2837–2852, https://doi.org/10.5194/acp-11-2837-2011, 2011.

Lambe, A. T., et al.: Relationship between oxidation level and optical properties of secondary organic aerosol, Environ. Sci. Technol., 47, 6349–6357, https://doi.org/10.1021/es401043j, 2013.

Law, K. S., Roiger, A., Thomas, J. L., Marelle, L., Raut, J.-C., Dalsoren, S., Fuglestvedt, J., Tuccella, P., Weinzierl, B., Schlager, H.: Local Arctic air pollution: Sources and impacts. Ambio, 46, doi:10.1007/s13280-017-0962-2, 2017.

Laskin, A., Laskin, J., and Nizkorodov, S. A.: Chemistry of Atmospheric Brown Carbon, Chem. Rev., 115, 4335–4382, https://doi.org/10.1021/cr5006167, 2015.

Lesins, G., Chylek, P., and Lohmann, U.: A study of internal and external mixing scenarios and its effect on aerosol optical properties and direct radiative forcing, J. Geophys. Res., 107, 4094, https://doi.org/10.1029/2001JD000973, 2002.

Lin, G., Penner, J. E., Flanner, M. G., Sillman, S., Xu, L., Zhou, C.: Radiative forcing of organic aerosol in the atmosphere and on snow: Effects of SOA and brown carbon, J. Geophys. Res., 119, 7453–7476, https://doi.org/10.1002/2013JD021186, 2014.

Liu, H. Y., Jacob, D. J.; Bey, I, Yantosca, R. M.: Constraints from Pb-210 and Be-7 on wet deposition and transport in a global three-dimensional chemical tracer model driven by assimilated meteorological fields, J. Geophys. Res., 106, 12109–12128, doi:10.1029/2000jd900839, 2001.

Liu, J., Fan, S., Horowitz, L. W., Levy II, H.: Evaluation of factors controlling long-range transport of black carbon to the Arctic, J. Geophys. Res., 116, https://doi.org/10.1029/2010JD015145, 2011.

Lukács, H., Gelencsér, A., Hammer, S., Puxbaum, H., Pio, C., Legrand, M., Kasper-Giebl, A., Handler, M., Limbeck, A., Simpson, A.: Seasonal trends and possible sources of brown carbon based on 2-year aerosol measurements at six sites in Europe, J. Geophys. Res., 112, https://doi.org/10.1029/2006JD008151, 2007.

Mahowald, N. M., Kloster, S., Engelstaedter, S., Moore, J. K., Mukhopadhyay, S., McConnell, J. R., Albani, S., Doney, S. C., Bhattacharya, A., Curran, M. A. J., Flanner, M. G., Hoffman, F. M., Lawrence, D. M., Lindsay, K., Mayewski, P. A., Neff, J., Rothenberg, D., Thomas, E., Thornton, P. E., and Zender, C. S.: Observed 20th century desert dust variability: impact on climate and biogeochemistry, Atmos. Chem. Phys., 10, 10875–10893, https://doi.org/10.5194/acp-10-10875-2010, 2010.

Mie, G.: Beiträge zur Optik trüber Medien, speziell kolloidaler Metallösungen, Ann. Phys., 330, 377–445, 1908.

Painter, T. H., Deems, J. S., Belnap, J., Hamlet, A. F., Landry, C. C., Udall, B.: Response of Colorado River runoff to dust radiative forcing in snow, PNAS, 107 (40), 17125-17130, https://doi.org/10.1073/pnas.0913139107, 2010.

670 Park, R. J., Jacob, D. J., Chin, M., Martin, R. V.: Sources of carbonaceous aerosols over the United States and implications for natural visibility, J. Geophys. Res., 108, 4355, https://doi.org/10.1029/2002JD003190, 2003.

Petzold, A., et al.: Saharan dust absorption and refractive index from aircraft-based observations during SAMUM 2006, Chemical and Physical Meteorology, 61, 118–130, https://doi.org/10.1111/j.1600-0889.2008.00383.x, 2009.

Pitari, G., Di Genova, G., Coppari, E., De Luca, N., Di Carlo, P., Iarlori, M., and Rizi, V.: Desert dust transported over Europe:
675 Lidar observations and model evaluation of the radiative impact, J. Geophys. Res., 120, 2881–2898, doi:10.1002/2014JD022875, 2015.

Pitari, G., Di Genova, G., De Luca, N.: A Modelling Study of the Impact of On-Road Diesel Emissions on Arctic Black Carbon and Solar Radiation Transfer, Atmosphere, 6, 318–340, https://doi.org/10.3390/atmos6030318, 2015.

Pye, H. O. T., Chan, A. W. H., Barkley, M. P., and Seinfeld, J. H.: Global modeling of organic aerosol: the importance of
680 reactive nitrogen (NO_x and NO_3), Atmos. Chem. Phys., 10, 11261–11276, https://doi.org/10.5194/acp-10-11261-2010, 2010.

Ridley, D. A., Heald, C. L., Ford, B.: North African dust export and deposition: a satellite and model perspective, J. Geophys. Res., 117, https://doi.org/10.1029/2011JD016794, 2012.

Rienecker, M. M., et al.: MERRA: NASA's modern era retrospective analysis for research and applications, J. Climate, 24, 3624–3648, https://doi.org/10.1175/JCLI-D-11-00015.1, 2011.

685 Saleh, R., Marks, M., Heo, J., Adams, P. J., Donahue, N. M., Robinson, A. L.: Contribution of brown carbon and lensing to the direct radiative effect of carbonaceous aerosols from biomass and biofuel burning emissions, J. Geophys. Res.-Atmos., 120, 10285–10296, https://doi.org/10.1002/2015JD023697, 2015.

Schär, C. and N. Kröner, N.: Sequential Factor Separation for the Analysis of Numerical Model Simulations, J. Atmos. Sci., 74,1471–1484, https://doi.org/10.1175/JAS-D-16-0284.1, 2017.

690 Sinyuk, A., Torres, O., Dubovik, O.: Combined use of satellite and surface observations to infer the imaginary part of refractive index of Saharan dust, Geophys. Res. Lett., 30, doi: 10.1029/2002GL016189, 2003.

Skiles, S. M., Painter, T. H., Deems, J., Landry, C., Bryant, A.: Dust radiative forcing in snow of the Upper Colorado River Basin. Part II: interannual variability in radiative forcing and snowmelt rates, Water Resour. Res., 48, W07522, https://doi.org/10.1029/2012WR011986, 2012.

695 Skiles, S. M., Flanner, M., Cook, J. M., Dumont, M., Painter, T. H.: Radiative forcing by light-abosorbing particles in snow, Nature Climate Change, 8, 964–971, https://doi.org/10.1038/s41558-018-0296-5, 2018.

Sturm, M., Goldstein, M. A., Parr, C.: Water and life from snow: a trilliondollar science question. Water Resour. Res., 53, 3534–3544, https://doi.org/10.1002/2017WR020840, 2017.

Tegen, I., Werner, M., Harrison, S. P., Kohfeld, F. E.: Relative importance of climate and land use in determinating present and future global soil dust emissions, Geophys. Res. Lett., 31, https://doi.org/10.1029/2003GL019216, 2004.

Tuccella, P., Thomas, J. L., Law, K. S., Raut, J.-C., Marelle, L., Roiger, A., Weinzierl, B., Denier van der Gon, H. A. C., Schlager, H., Onishi, T.: Air pollution impacts due to petroleum extraction in the Norwegian Sea during the ACCESS aircraft campaign, Elem. Sci. Anth., 5, p.25., http://doi.org/10.1525/elementa.124, 2017.

Tuccella, P., Curci, G., Pitari, G., Lee, S., Jo, D. S.: Direct radiative effect of absorbing aerosols: sensitivity to mixing state, brown carbon and dust refractive index and shape, J. Geophys. Res., 125, e2019JD030967, https://doi.org/10.1029/2019JD030967, 2020.

Updyke, K. M., Nguyen, T. B., Nizkorodov, S. A.: Formation of brown carbon via reactions of ammonia with secondary organic aerosols from biogenic and anthropogenic precursors, Atmos. Env, 63, 22–31, https://doi.org/10.1016/j.atmosenv.2012.09.012, 2012.

van der Werf, G. R., Randerson, J. T., Giglio, L., Collatz, G. J., Mu, M., Kasibhatla, P. S., Morton, D. C., DeFries, R. S., Jin, Y., and van Leeuwen, T. T.: Global fire emissions and the contribution of deforestation, savanna, forest, agricultural, and peat fires (1997–2009), Atmos. Chem. Phys., 10, 11707–11735, https://doi.org/10.5194/acp-10-11707-2010, 2010.

Wagner, R., Ajtai, T., Kandler, K., Lieke, K., Linke, C., Müller, T., Schnaiter, M., and Vragel, M.: Complex refractive indices of Saharan dust samples at visible and near UV wavelengths: a laboratory study, Atmos. Chem. Phys., 12, 2491–2512, https://doi.org/10.5194/acp-12-2491-2012, 2012.

Wang, X., Doherty, S. J., Huang, J.: Black carbon and other light-absorbing impurities in snow across North China. J. Geophys. Res., 118, 1471–1492, https://doi.org/10.1029/2012JD018291, 2013.

Wang, X., Heald, C. L., Ridley, D. A., Schwarz, J. P., Spackman, J. R., Perring, A. E., Coe, H., Liu, D., and Clarke, A. D.: Exploiting simultaneous observational constraints on mass and absorption to estimate the global direct radiative forcing of black carbon and brown carbon, Atmos. Chem. Phys., 14, 10989–11010, https://doi.org/10.5194/acp-14-10989-2014, 2014.

Wang, X., Heald, C. L., Sedlacek, A. J., de Sá, S. S., Martin, S. T., Alexander, M. L., Watson, T. B., Aiken, A. C., Springston, S. R., and Artaxo, P.: Deriving brown carbon from multiwavelength absorption measurements: method and application to AERONET and Aethalometer observations, Atmos. Chem. Phys., 16, 12733–12752, https://doi.org/10.5194/acp-16-12733-2016, 2016.

725 Wang, X., Heald, C. L., Liu, J., Weber, R. J., Campuzano-Jost, P., Jimenez, J. L., Schwarz, J. P., and Perring, A. E.: Exploring the observational constraints on the simulation of brown carbon, Atmos. Chem. Phys., 18, 635–653, https://doi.org/10.5194/acp-18-635-2018, 2018.

Ward, J. L., Flanner, G. M., Bergin, M., Dibb, J. E., Polashenski, C. M., Soja, A. J., Thomas, J. L.: Modeled response of Greenland snowmelt to the presence of biomass burning-based absorbing aerosol in the atmosphere and snow, J. Geophys.
730 Res., 123, 6122–6141, https://doi.org/10.1029/2017JD027878, 2018.

Warren, S., Clarke, A.: Soot in atmosphere and snow surface of Antarctica. J. Geophys. Res., 95D2, 1811–1816, https://doi.org/10.1029/JD095iD02p01811, 1990.

Warren, G. S.: Light-absorbing impurities in snow: a personal and historical account, Front. Earth Sci., 6:250, https://doi.org/10.3389/feart.2018.00250, 2019.

735 Wu, C., Liu, X., Lin, Z., Rahimi-Esfarjani, S. R., Lu, Z.: Impacts of absorbing aerosol deposition on snowpack and hydrologic cycle in the Rocky Mountain region based on variable-resolution CESM (VR-CESM) simulations, Atmos. Chem. Phys., 18, 511–533, https://doi.org/10.5194/acp-18-511-2018, 2018.

Ye, H., Zhang, R., Shi, J., Huang, J., Warren, S. G., Fu, Q.: Black carbon in seasonal snow across northern Xinjiang in northwestern China, Environ. Res. Lett., 7, doi:10.1088/1748-9326/7/4/044002, 2012.

740 Zhao, S., Jiang, T., Wang, Z.: Snow grain-size estimation using Hyperion Imagery in a typical area of the Heihe River Basin, China, Remote sens., 5, 238–253, doi:10.3390/rs5010238, 2013.

Zatko, M. C., Warren, S. G.: East Antarctic sea ice in spring: spectral albedo of snow, nilasm frost flowers5 and slush, and light-absorbing impurities in snow, Annals of Glaciology, 56, 10.3189/2015AoG69A574, 2015.

Zender, C. S., Bian, H., Newman, D.: Mineral Dust Entrainment and Deposition (DEAD)model: Description and 1990s dust
745 climatology, J. Geophys. Res., 108, https://doi.org/10.1029/2002JD002775, 2003.

Zhang, L. M., Gong, S. L., Padro, J., Barrie, L.: A sizesegregated particle dry deposition scheme for an atmospheric aerosol module, Atmos. Environ., 35, 2549–560, https://doi.org/10.1016/S1352-2310(00)00326-5, 2001.

Zhang, Y., et al.: Top-of-atmosphere radiative forcing affected by brown carbon in the upper troposphere, Nature Geoscience, 10, 486–489, doi:10.1038/ngeo2960, 2017.

750

Tables

Table 1. Summary of the numerical experiments.

Experiment	Description
CTRL[1]	Control run, reference scenario. Mid absorption.
OSPT[1]	RF calculated separately for each RAA
BC-H[1]	High absorption, aged BC E_{abs}=1.9
BC-L[1]	Low absorption, aged BC E_{abs}=1.1
BrC-H[1]	High absorption, no blanching for aged BB BrC
BrC-L[1]	Low absorption, blanching for aged BF BrC
DUST-H[1]	High absorption, dust refractive index from Wagner et al. (2012)
DUST-L[1]	Low absorption, dust refractive index from Sinyuk (2003)
BCE-H[2]	BCE doubled
BCE-L[2]	BCE halved
R_e-H[2]	Snow grain size multiplied by 2
R_e-L[2]	Snow grain size divided by 2
SCF-H[2]	Snow coverage fraction increased by 1.5
SCF-L[2]	Snow coverage fraction decreased by 1.5

755   [1]MACs adopted for these experiments are reported in Table 2.

[2]MACs adopted for these experiments are the same one of CTRL (Table 2).

Table 2. Summary of the MACs in visible band[1] used in the experiments. The units are in m^2/g.

Experiment	MAC adopted for each radiation-absorbing aerosol species			
	Fresh FF BC	Aged FF BC	Fresh BF/BB BC	Aged BF/BB BC
CTRL	6.5	9.8	6.2	9.3
BC-H	6.5	12.4	6.2	11.8
BC-L	6.5	7.2	6.2	6.8
	Fresh BF BrC	Aged BF BrC	Fresh BB BrC	Aged BB BrC
CTRL	1.1	1.1	1.7	0.71
BrC-H	1.1	1.1	1.7	1.7
BrC-L	1.1	0.46	1.7	0.71
	Dust 0.36–0.6	Dust 2.6–3.6	Dust 4.4–6.0	Dust 7.0–12.0
CTRL	0.085	0.059	0.048	0.039
DUST-H	0.14	0.086	0.067	0.052
DUST-L	0.037	0.029	0.025	0.021

[1]MACs reported here are spectrally averaged spectrally averaged between 0.3-0.7 μm over an incident solar spectrum characteristic of summer high-latitude conditions.

[2]The experiment list is reported in Table 1.

Table 3. Global all-sky annual mean surface snow RF (W/m^2) of total RAAs, BC, BrC, and mineral dust calculated in the experiments discussed in Section 2.4 (see also Table 1). The percentages represent the deviations from CTRL run.

Experiment	All RAAs	BC	BrC	Dust
CTRL	+0.068	+0.033	+0.0066	+0.012
OSPT[1]	+0.089 (+31%)	+0.049 (+48%)	+0.018 (+167%)	+0.023 (+92%)
BC-H	+0.073 (+8%)	+0.038 (+16%)	+0.0059 (-11%)	+0.011 (-10%)
BC-L	+0.062 (-9%)	+0.027 (-18%)	+0.0073 (+10%)	+0.013 (+5%)
BrC-H	+0.071 (+4%)	+0.032 (-2%)	+0.0095 (+44%)	+0.012 (-)
BrC-L	+0.067 (-2%)	+0.034 (+4%)	+0.0051 (-22%)	+0.012 (-)
DUST-H	+0.071 (+5%)	+0.032 (-4%)	+0.0059 (-11%)	+0.015 (+25%)
DUST-L	+0.063 (-7%)	+0.035 (+5%)	+0.0071 (+8%)	+0.0072 (-40%)
BCE-H	+0.10 (+52%)	+0.050 (+50%)	+0.0095 (+44%)	+0.017 (+40%)
BCE-L	+0.044 (-36%)	+0.021 (-36%)	+0.0037 (-44%)	+0.0078 (-35%)
R_e-H	+0.092 (+36%)	+0.045 (+36%)	+0.0088 (+33%)	+0.016 (+30%)
R_e-L	+0.050 (-27%)	+0.024 (-27%)	+0.0051 (-22%)	+0.0090 (-25%)
SCF-H	+0.088 (+29%)	+0.043 (+29%)	+0.0081 (+22%)	+0.016 (+30%)
SCF-L	+0.058 (-15%)	+0.029 (-13%)	+0.0059 (-11%)	+0.0096 (-20%)
Total Uncertain[2]	0.035- 0.12	0.017-0.059	0.0028-0.019	0.0044-0.025
	-49%/+77%	-50%/+61%	-57%/+183%	-63%/+112%

[1]For this experiment, total RAAs snow RF was calculated as the sum of the single species.

[2] The lower and upper bounds were calculated by adding in quadrature the RF from each experiment.

770 **Table 4. Domain of the regions used in this study.**

Region	Longitude range	Latitude range
Arctic	60°N - 90 °N	-180°E – 180°E
Nord America	29°N – 60°N	-155°E – 60°E
Europe	40°N – 60°N	-10°E – 45°E
Asia	25°N – 60°N	45°E – 160°E
Antarctica	90°S – 60°S	-180°E – 180°E
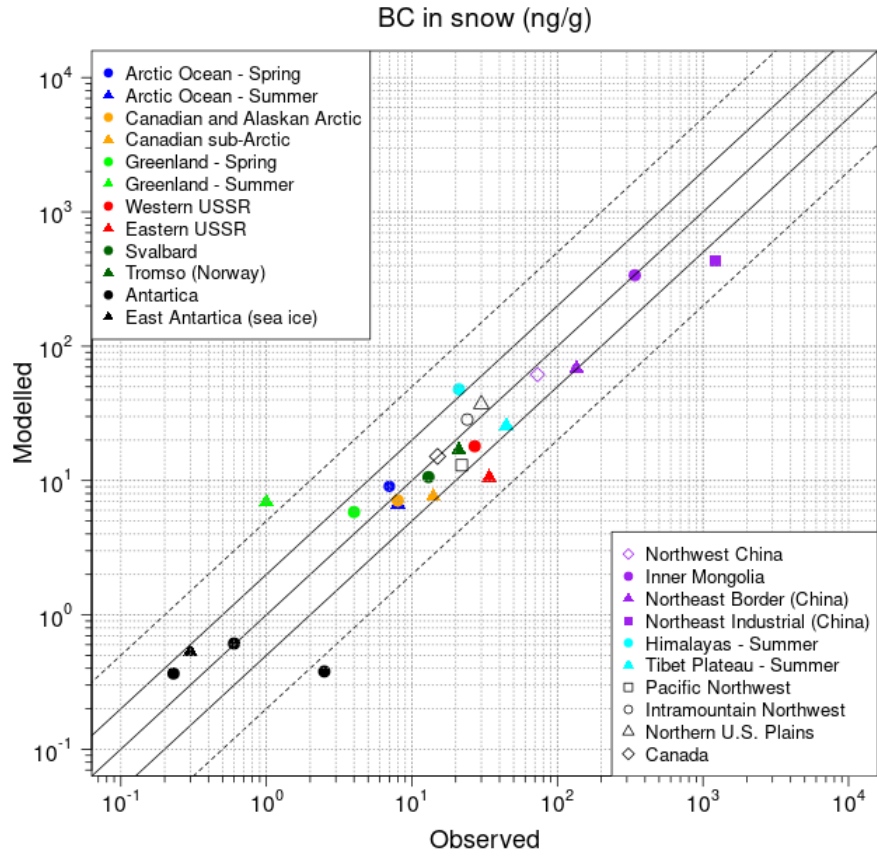
Figure 1: Scatter plots of the observed and modelled BC mixing ratio in the snow. Central continue line is the 1:1 line, other continue lines correspond to 1:2 and 2:1 lines. Dotted lines correspond to 1:5 and 5:1 lines.
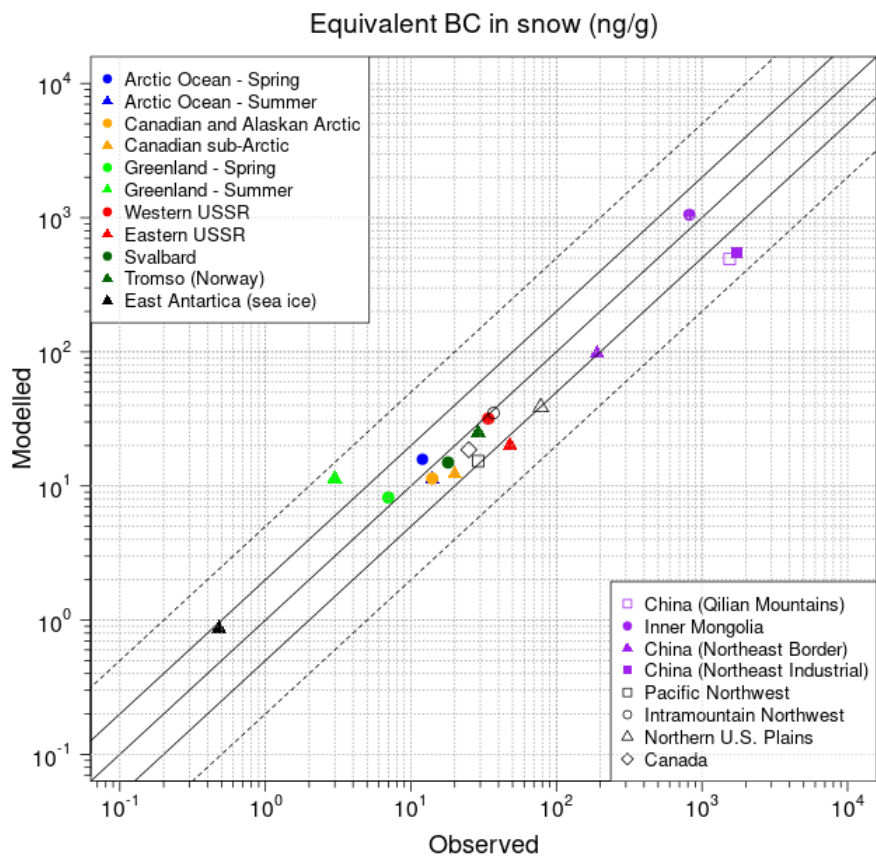
780

Figure 2. Same as Figure 1, but for black carbon equivalent (BCE). BCE is defined in Equation 2 and represents the RAA snow mass scaled with the MAC of each species.
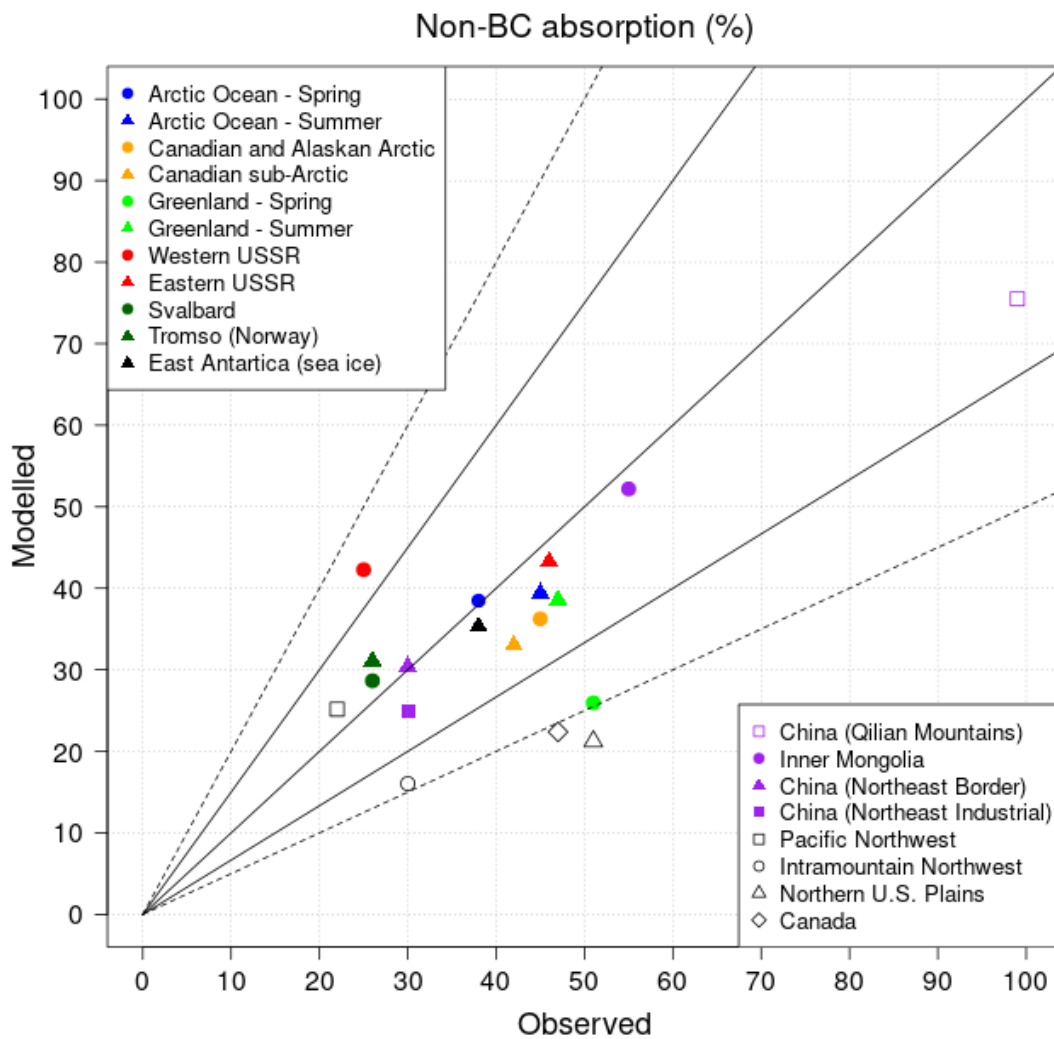
785

Figure 3: Scatter plots of the observed and modelled $f_{\text{non-BC}}$ in the snow. Central continue line is the 1:1 line, other continue lines correspond to 1:1.5 and 1.5:1 lines. Dotted lines correspond to 1:2 and 2:1 lines. Non-BC means the sum of BrC and dust (reported to BC equivalent).
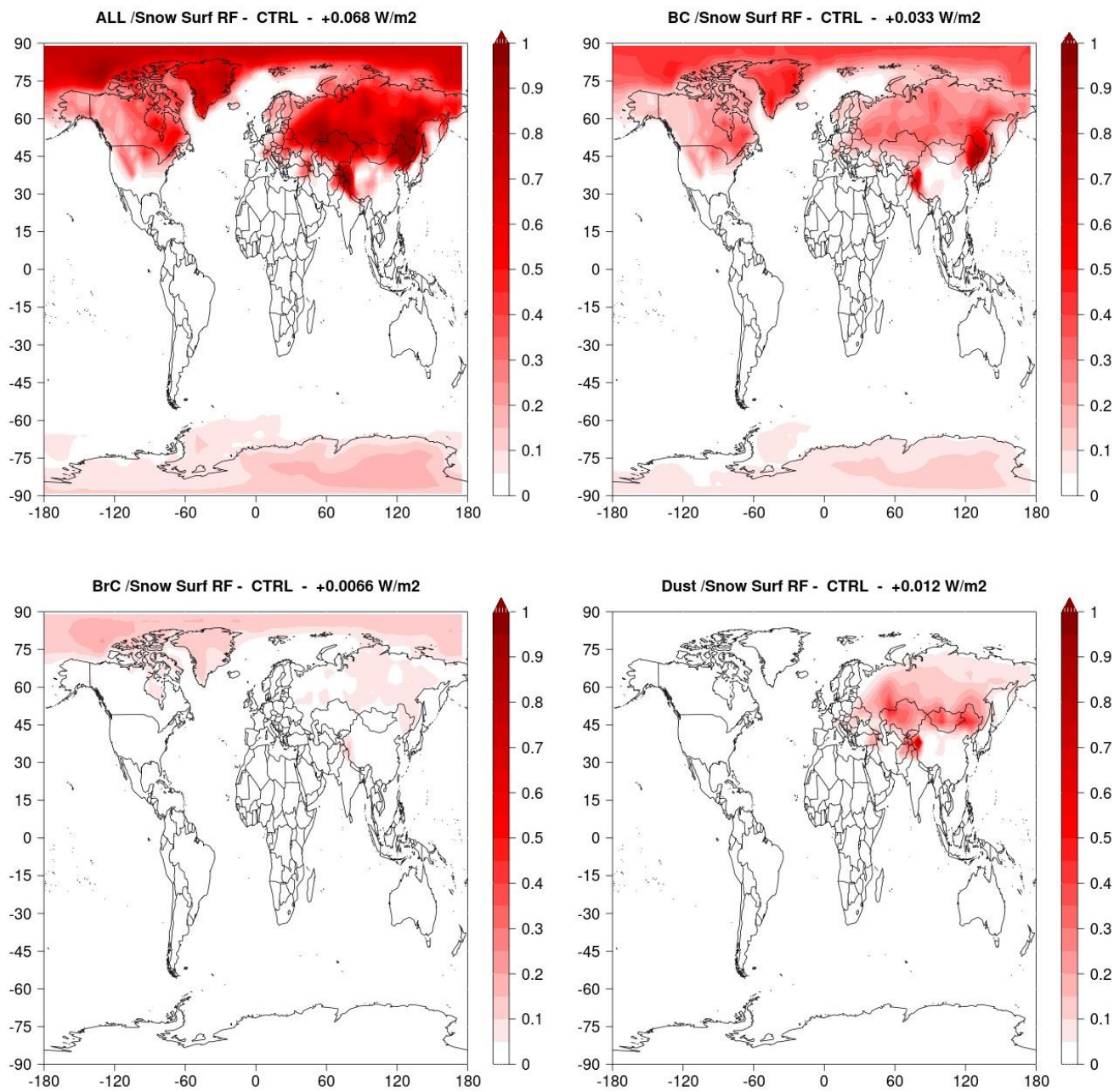
790

Figure 4. All-sky annual mean (2010–2014) radiation-absorbing aerosols (RAA), black carbon (BC), brown carbon (BrC), and soil dust in snow radiative forcing (RF) calculated from CTRL experiment.
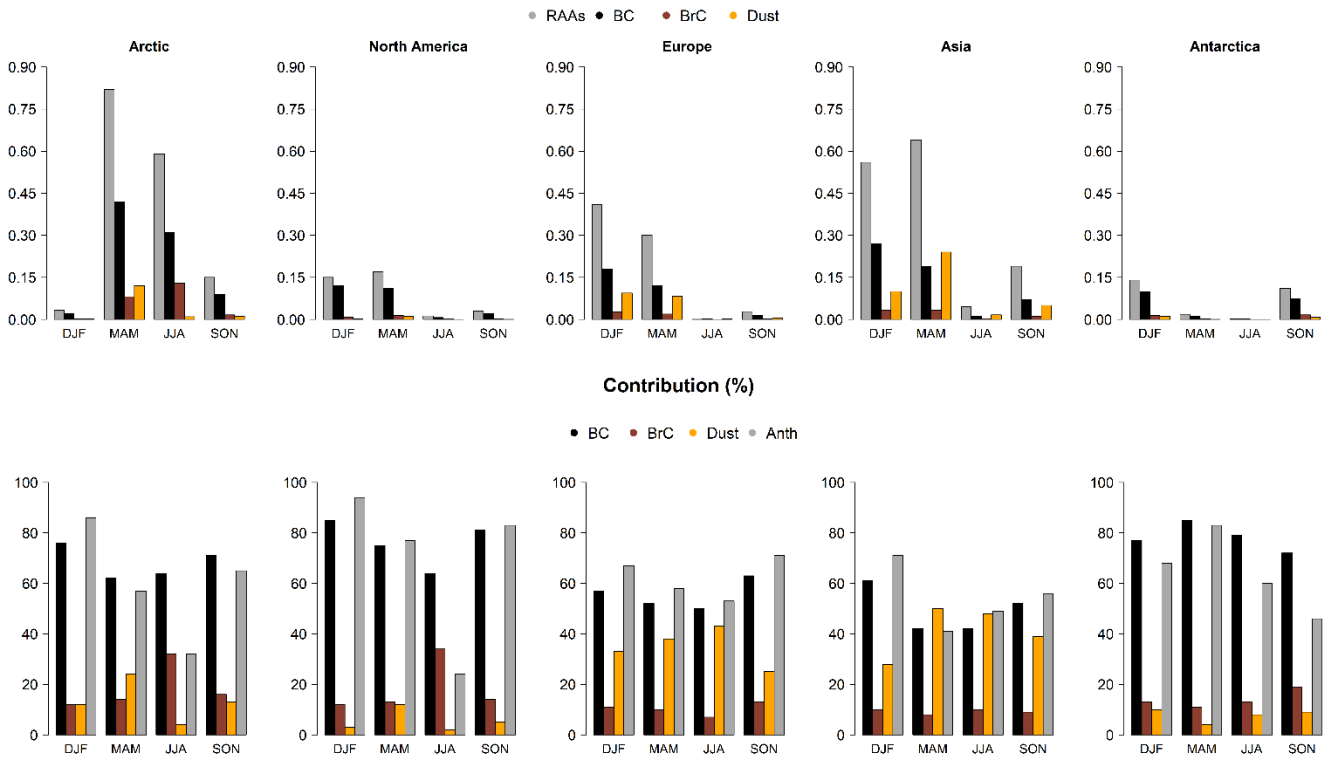
795 **Figure 5. Top panel: all-sky regional and seasonal averages (2010–2014) (top panel) of total RAAs, black carbon (BC), brown carbon (BrC), and soil dust snow radiative forcing (RF), calculated from CTRL experiment in Arctic, North America, Europa, Asia, and Antarctica. Bottom panel: contribution of each single species and anthropogenic RAA to total forcing. The anthropogenic contribution is given by BC and BrC from fossil fuel (FF) and biofuel (BF) sources and aromatic SOA.**